

Writing Programmable Schottky Diodes in MoS₂ Transistors via Nanoscale Ferroelectric Control

Zhiyong Xiao, Jingfeng Song, Stephen Ducharme and Xia Hong*

Department of Physics and Astronomy and Nebraska Center for Materials and Nanoscience,
University of Nebraska-Lincoln, Nebraska 68588-0299, USA

*: xhong2@unl.edu

Abstract:

The nonvolatile, nanoscale controllable polarization of a ferroelectric gate offers unique opportunities to induce local potential variation and impose designed functionalities in two-dimensional materials such as atomically thin transition metal dichalcogenides. In this work, we employ scanning probe microscopy to control the domain structures in an ultrathin ferroelectric polymer top-gate, which induces three distinct electronic states in a monolayer MoS₂ field effect device with a SiO₂ global back-gate: the high conductance ON state, low conductance OFF state, and a diode state with a rectified source-drain current versus voltage characteristic. The induced nonlinear conduction can be well described by the thermionic emission model, with the Schottky barrier height varying from 0.38 eV to 0.57 eV, which can be further tuned by the back-gate voltage. Our study paves the way for the rational design of reconfigurable homojunctions and nanostructures in van der Waals materials for novel multifunctional nanoelectronic and optoelectronic applications.

The ever-increasing demand on the information storage and data processing capacities for modern electronics calls for new material platforms and device concepts to transcend the fundamental scaling limitations faced by the conventional semiconductor technology [1]. Promising solutions being actively investigated include incorporating nanoscale or low-dimensional materials [2-4], creating three-dimensional circuit architectures [2], and embedding reconfigurable functionalities in a single device [4, 5]. Among the various nanoscale electronic systems, the two-dimensional (2D) transition metal dichalcogenides (TMDCs) (MX_2 with $M = Mo, W$ and $X = S, Se, Te$) possess highly tunable electronic states that can be controlled via the electric field effect [6, 7]. The atomic thickness and the direct band gaps of 1-2 eV for monolayer (ML) TMDCs make them a promising candidate for building nanoelectronic [8-11] and optical devices [12-14]. In addition to the field effect transistor (FET), an essential element for logic and optoelectronic applications is the Schottky or p-n junction device with well-defined barrier height and controlled photo-response. In previous studies, TMDC-based junction devices have been demonstrated by employing multiple local gates [14, 15], electric-double-layer gating controlled bipolar carrier injection [16], contact work function engineering [17, 18], or heterojunctions formed between different van der Waals materials [19-22]. In all of these studies, the device functions are not reconfigurable after fabrication.

A promising approach to induce local potential confinement and produce a programmable junction state in TMDCs is to capitalize on the nonvolatile, switchable polarization field of a ferroelectric gate. The ferroelectric field effect has previously been intensively investigated in 2D materials such as graphene and TMDCs for building novel logic and memory devices [5, 23-25], tunnel junctions [26], sensors [27-29], and plasmonic and optoelectronic applications [30-32]. To date, however, the unique opportunity offered by the nanoscale ferroelectric domain patterning, which can lead to local carrier density modulation in the 2D channel, has

not been explored. In this study, we report a multifunctional MoS₂ device with programmable transistor and Schottky junction states via scanning probe control of the domain structures in a ferroelectric top-gate. Figure 1a shows the schematic diagram of a MoS₂ FET sandwiched between a SiO₂ global back-gate and a ferroelectric polymer top-gate. We employ conductive probe atomic force microscopy (AFM) and piezo-response force microscopy (PFM) to write and image nanoscale ferroelectric domain patterns in the copolymer poly(vinylidene fluoride-trifluoroethylene) [P(VDF-TrFE)] top layer, which has induced controlled switching among three distinct electronic states in the MoS₂ channel. When the out-of-plane polarization is uniformly switched to the up (P_{up}) or down (P_{down}) orientation, MoS₂ exhibits low conductance OFF or high conductance ON states, respectively. For both states, the source-drain current (I_{DS}) versus voltage (V_{DS}) characteristic is linear, reflecting ohmic conduction. In sharp contrast, when the copolymer is polarized into two adjacent ferroelectric domains with opposite out-of-plane polarization directions (denoted as the half P_{up} - half P_{down} state), the MoS₂ channel exhibits a diode-like rectified $I_{\text{DS}}-V_{\text{DS}}$ behavior that can be well described by the thermionic emission model. The barrier height of the induced Schottky junction varies from 0.38 eV to 0.57 eV and can be further controlled by the back-gate voltage (V_{bg}). Our work facilitates the development of TMDC-based integrated circuits with programmable functionalities for nanoelectronic and optoelectronic applications.

Device characterization

We deposited 10 MLs (17.8 ± 0.7 nm) of P(VDF-TrFE) films on top of ML MoS₂ devices fabricated on 300 nm SiO₂ substrates using the Langmuir-Blodgett (LB) technique (Materials and Methods) [33, 34]. Previous studies of the ferroelectric polymer-2D hybrid devices have focused on spin-coated films [5, 23, 27, 32], where the resulting films are typically thicker than 100 nm. The corresponding coercive voltages are >50 V, well exceeding what can be supplied by a conductive AFM probe. The surface morphology of these films is generally

very rough, not suitable for controlled scanning probe writing. In contrast, the LB technique can yield ultrathin P(VDF-TrFE) films with smooth surfaces (about 1 nm surface roughness), which allows us to create ferroelectric domain patterns with nanoscale precision in the copolymer top-gate using a conductive AFM tip [35, 36]. Figures 1b-c show the Raman and photoluminescence (PL) spectra of a typical ML MoS₂ sample, where no pronounced changes are observed upon the deposition of the ferroelectric top layer. Figure 1d shows the transfer characteristic of device D1 controlled by the SiO₂ back-gate, where I_{DS} increases with increasing V_{bg} , suggesting the MoS₂ channel is intrinsically *n*-doped. This device possesses a field effect mobility (μ_{FE}) of 6.2 cm²V⁻¹s⁻¹, and a subthreshold swing of 2-3 V dec⁻¹, consistent with those reported in previous studies [11]. The device exhibits an exponential I_{DS} growth at low V_{bg} followed by a quasi-linear gate dependence at high V_{bg} , signaling the shift of the Fermi level E_F from well residing in the bandgap regime to close to the conduction band edge. We define the critical voltage where I_{DS} - V_{bg} deviates from the exponential behavior as the transition voltage (V_t), which shifts from -16 V for the bare sample to +15 V after the P(VDF-TrFE) deposition (Fig. 1d). This corresponds to a decrease in the electron density of about 2×10^{12} cm⁻² in MoS₂, which may be due to the encapsulation of an interfacial water adsorbate layer [37]. Despite the relatively high dielectric constant ($\kappa \sim 10$) of P(VDF-TrFE) [34], the presence of the ferroelectric polymer does not yield a significant change in the mobility and subthreshold swing of the device. It has been shown in previous studies that interfacing with a high- κ dielectric layer can effectively enhance the mobility of MoS₂ [9, 38]. Unlike conventional high- κ dielectrics such as Al₂O₃ and HfO₂, the ferroelectric polymer has a high spontaneous polarization that is mostly un-aligned in the as-grown state. We thus expect a high density of Coulomb impurities resulting from the spatially inhomogeneous bound charge density at the device interface, which can serve as a major scattering source and suppress the mobility of MoS₂. For the six MoS₂ devices reported

in this study, the mobility values range from 3 to 7 $\text{cm}^2\text{V}^{-1}\text{s}^{-1}$.

Nonvolatile ferroelectric polarization control of MoS₂ FET

We first investigated the ferroelectric field effect in the MoS₂ FET. Figure 2a shows the room temperature transfer characteristics of device D2 at different poling states of the ferroelectric top-gate. In the as-grown state, the device exhibits a mobility of $\mu_{\text{FE}} = 6.7 \text{ cm}^2\text{V}^{-1}\text{s}^{-1}$ with $V_t = -20 \text{ V}$. To control the out-of-plane polarization of the ferroelectric polymer, we apply a constant bias voltage higher than the coercive voltage to a conductive AFM tip while it is scanning on the sample surface in the contact mode. The details of this technique can be found in Refs. [35, 36] and the Materials and Methods section. In the first poling, we switched the ferroelectric gate to the P_{down} state by writing the entire channel area (Fig. 2b) with the tip bias V_{tip} of +10 V and keeping the MoS₂ sample grounded. Figure 2c shows the PFM phase image of the resulting domain structure. Only the copolymer film deposited on top of the MoS₂ device has been uniformly polarized, while the rest of the area deposited on the SiO₂ substrate remains unpoled. In the P_{down} state, electrons are accumulated in the MoS₂ channel, which shifts the Fermi level towards the conduction band edge, yielding a nonvolatile offset in the doping level. The resulting transfer curve shifts to the negative V_{bg} direction, with a lower V_t of -38 V. The corresponding mobility is $4.7 \text{ cm}^2\text{V}^{-1}\text{s}^{-1}$ in this state.

We then polarized the ferroelectric top-gate to the uniform P_{up} state (Fig. 2d) by writing the entire device area with $V_{\text{tip}} = -10 \text{ V}$, depleting electrons from MoS₂. The resulting $I_{\text{DS}}-V_{\text{bg}}$ curve shifts to the positive V_{bg} direction with $V_t = -12 \text{ V}$. The mobility in this state is $3.3 \text{ cm}^2\text{V}^{-1}\text{s}^{-1}$, slightly lower than that for the P_{down} state. This may result from a slight polarization asymmetry in P(VDF-TrFE) that energetically favors the P_{down} state, which can lead to a higher density of disordered bound charge in the P_{up} state. Such polarization asymmetry has previously been observed in P(VDF-TrFE) films prepared on Au substrates [36].

The scanning probe controlled polarization switching is nonvolatile and fully reversible. After the third AFM writing with $V_{\text{tip}} = +10$ V, we polarized the polymer back to the P_{down} state, and the transfer curve of MoS₂ overlaps with that after the first poling. The high conductance (P_{down}) and low conductance (P_{up}) states of the device can thus be used to represent the “ON” and “OFF” states for non-volatile memory operations, respectively, with the current switching ratio reaching 450 at $V_{\text{bg}} = -25$ V. Despite the large ratio of current modulation, we observe ohmic conduction for both P_{up} and P_{down} states over the entire gating range for all devices investigated. Figure 3a shows the I_{DS} versus V_{DS} curves taken on device D3 at $V_{\text{bg}} = -10$ V, which exhibit linear behaviors for both polarization states.

Programmable junction state in MoS₂ FET via ferroelectric domain patterning

We next explored the possibility of inducing a potential barrier in the MoS₂ channel by writing a ferroelectric domain wall (DW) perpendicular to the current direction in device D3 (Fig. 3b top inset), which separates two domains with opposite out-of-plane polarization directions. In sharp contrast with the results obtained in the uniformly polarized states (Fig. 3a), at the same gate voltage of -10 V, the device exhibits a much weaker variation in I_{DS} at the reverse-bias, consistent with a diode-type rectified nonlinear conduction. Such nonlinearity can be further tuned by the back-gate voltage. Figure 3b shows a plot of the color contour of normalized I_{DS} , defined as $I_{\text{DS}}/I_{\text{DS}}(V_{\text{DS}} = +100 \text{ mV})$, versus V_{DS} and V_{bg} for this device. There is a clear evolution of the I - V characteristic between two distinct behaviors with increasing V_{bg} . At low V_{bg} , labeled as region I, we observe a linear I - V relationship, resembling an ohmic-like resistor. At an intermediate gate voltage range (region II: $-12.5 \text{ V} \leq V_{\text{bg}} \leq 0 \text{ V}$), I_{DS} exhibits the diode-like rectified I_{DS} - V_{DS} relationship. Further increasing V_{bg} to region III recovers the linear conduction.

To understand the origin of the evolved I_{DS} - V_{DS} characteristic, we superimposed on Fig. 3b the transfer curves of this device in the uniformly polarized states. The corresponding

transition voltages are $V_t = -13$ V for the P_{down} state and $V_t = 0$ V for the P_{up} state, which are in excellent agreement with the boundary V_{bg} s that separate regions I, II, and III, suggesting that it is the band alignment in the half P_{up} -half P_{down} state that determines the channel conduction characteristic. When the device is gated in region I, both sides of the channel are in the semiconducting state, leading to high channel resistance. We can model the channel conduction as two resistors, a resistor R_{on} corresponding to the P_{down} domain and a resistor R_{off} corresponding to the P_{up} domain, in series connection (Fig. 3b bottom inset). The transport in both regions is dominated by thermally activated electrons, and we expect an n - n type interface where the ohmic-type conduction is preserved. Similarly, in region III, both channels are in the conducting state, yielding low channel resistance with linear conduction. However, in region II, where half of the channel is in the conducting state and the other half of the channel is in the semiconducting state, we expect a Schottky junction formed at the interface, with the barrier height corresponding to the difference in E_F for the P_{up} and P_{down} states (Fig. 4a).

Discussion

We quantitatively modeled the diode-like rectified I - V characteristic in region II using the thermionic emission model [39, 40]:

$$I_{DS} = A_{2D}^* T^{3/2} W \exp\left(-\frac{q\phi_B^{\text{eff}}}{k_B T}\right) \exp\left(\frac{qV_{DS}}{nk_B T}\right) \left[1 - \exp\left(-\frac{qV_{DS}}{k_B T}\right)\right] \quad (1)$$

$$\text{with } A_{2D}^* = \left[\frac{(qM_c k_B^{3/2})}{(\pi\hbar^2)}\right] (m_t^*/2\pi)^{1/2},$$

where W is the width of the conduction channel, q is the electron charge, ϕ_B^{eff} is the effective Schottky barrier, n is the ideality factor, which is normally between 1 and 2, and $m_t^* = 0.45m_0$ is the transverse electron effective mass for ML MoS₂ [8]. Here A_{2D}^* is the 2D effective Richardson constant, with the number of equivalent conduction band minima $M_c = 2$. Figures 4b-c show the I_{DS} - V_{DS} curves taken on device D4 in region II (between $V_{\text{bg}} = -12$ V and 0 V for this device). At $V_{\text{bg}} = -10$ V, the source-drain conduction characteristic can be

well described by Eq. (1) with $\phi_B^{\text{eff}} = 0.51 \text{ eV}$. For the four devices investigated (D3-D6), the effective Schottky barrier height ϕ_B^{eff} varies from 0.36 eV to 0.56 eV as controlled by V_{bg} . The ideality factor n ranges from 1.5 to 1.8, consistent with previously reported results [14, 17]. We thus demonstrated a prototype Schottky diode with well-defined barrier height via scanning probe writing of the half P_{down} -half P_{up} domain structure in the ferroelectric gate.

In region II, with the presence of the interface junction, we need to consider three circuit components in series connection to model the channel conduction, the resistors R_{on} and R_{off} , and an additional diode-type device in the vicinity of the DW (Fig. 3b bottom inset). As the MoS₂ device exhibits more than one order of magnitude change in resistance for the two polarization states in this region (Figs. 2a and 3a), we can neglect R_{on} when modelling the total channel resistance. The fact that Eq. (1) can give an accurate description of the conduction characteristic indicates that the R_{off} contribution is also absent at $V_{\text{bg}} = -10 \text{ V}$. A possible scenario is that, at low carrier density, the width for the junction transition region is comparable with or larger than the channel length at the P_{up} side. This means that Eq. (1) would not provide a satisfactory fit to $I_{\text{DS}}-V_{\text{DS}}$ at sufficiently high V_{bg} , when the junction width decreases with increasing carrier density and becomes shorter than the associated channel length. Such deviation is indeed observed for data at $V_{\text{bg}} \geq -6 \text{ V}$. Rather, the conduction has to be modelled as a diode in series connection with a resistor:

$$V'_{\text{DS}} = V_{\text{DS}}(I_{\text{DS}}) + I_{\text{DS}}R_{\text{off}}. \quad (2)$$

Here $V_{\text{DS}}(I_{\text{DS}})$ follows the rectified $I-V$ relationship defined by Eq. (1). Figure 4c shows the fit for the $I_{\text{DS}}-V_{\text{DS}}$ curve at $V_{\text{bg}} = -4 \text{ V}$ to this model, where the first term yields a barrier height of $\phi_B^{\text{eff}} = 0.43 \text{ eV}$. The second term for the R_{off} fit corresponds to an off-state channel length of 23 nm, much shorter than the associated P_{up} domain length (350 nm), confirming that the P_{up} side junction width is comparable with the channel length at this density range.

As a control experiment, we erased the domain structure by thermally heating the sample

in vacuum to 80 °C, close to its Curie temperature, for 2 hours. After the thermal treatment, the copolymer film recovers its as-deposited state with polarization randomly orientated, which was attributed to the low DW energy for P(VDF-TrFE) [36] and the lack of screening charges in vacuum. As shown in Fig. 4d, the I_{DS} - V_{DS} curve at $V_g = -10$ V after thermal depolarization agrees well with that in the as-grown state, indicating that the observed diode state is resulting from the ferroelectric domain patterning and the sample quality is preserved during the polarization switching.

As the Schottky barrier height ϕ_B^{eff} is defined by the mis-alignment of the Fermi levels for the P_{down} and P_{up} states (Fig. 4a), it can be further tuned by V_{bg} as the P_{down} side of the device is approaching the conduction band edge. Figure 5 shows ϕ_B^{eff} as a function of the normalized back gate voltage $(V_{\text{bg}}-V_{\text{mid}})/V_{\text{w}}$ taken on devices D3-D6, where V_{mid} and V_{w} are the middle point and width of region II, respectively. For all four devices, ϕ_B^{eff} decreases with V_{bg} , changing by 90-150 meV. This reduction in ϕ_B^{eff} is a consequence of the high density of states of the MoS₂ conduction band. The V_{bg} range for region II only corresponds to a small modulation of the on state E_F by 4-10 meV. We also note that at the boundary between regions II and III, where the channel conduction can no longer be properly modeled by Eq. (2), the off state E_F is still 0.4-0.5 eV below the conduction band edge. Previous studies reveal the existence of an impurity band tail with high density of states in TMDCs due to lattice defects [11, 18], which can extend to up to 0.5 eV below the conduction band of MoS₂ [11]. These impurity states can contribute to hopping-type conduction, which naturally explains the lack of a well-defined energy barrier at this gating range.

Conclusion

In summary, we have demonstrated a prototype multifunctional MoS₂ device with nonvolatile, programmable transistor and diode states via local control of the ferroelectric domain structure in an ultrathin ferroelectric polymer top-gate. Our work reveals the rich

opportunities brought by combining the ferroelectric field effect with the scanning probe approach in the study of van der Waals materials, which paves the way for the rational design of functional homojunctions and nanostructures in the 2D channel and integrating programmable circuit elements in a single material platform for nanoelectronic and optoelectronic applications.

Materials and Methods:

Sample preparation

We mechanically exfoliated MoS₂ thin flakes from commercial bulk crystals (2Dsemiconductors Inc.) onto 300 nm SiO₂/*p*-doped Si substrates. The ML pieces were identified with Raman and PL spectroscopies using a Renishaw inVia Raman system with 514 nm laser wavelength. The difference between the Raman A_{1g} and E_{2g}¹ modes is about 19 cm⁻¹ (Fig. 1b) and the PL spectrum peaks at 18.4 eV (Fig. 1c). Selected ML MoS₂ flakes were fabricated into two-point devices via standard e-beam lithography followed by e-beam evaporation of 5 nm Ti/50 nm Au as the electrodes, which exhibit linear I_{DS}-V_{DS} behavior within the source-drain voltage range of 0.1 V before the deposition of the ferroelectric polymer top layer.

The ferroelectric copolymer P(VDF-TrFE) films were prepared by dissolving 70% vinylidene fluoride and 30% trifluoroethylene (Kunshan Hisense Electronics Co., Ltd.) in dimethylsulfoxide with a concentration of 0.05% by weight. Thin films of nominal 10 MLs (1.78±0.07 nm/ML) were transferred layer-by-layer onto the MoS₂ devices via the horizontal Langmuir-Blodgett deposition at a surface pressure of 5 mN/m [33, 34]. The LB films have smooth surfaces with root-mean-square surface roughness of about 1 nm, and the polarization is randomly oriented in the un-poled, as-grown state, as revealed by the PFM measurements. Upon the P(VDF-TrFE) deposition, both the E_{2g}¹ and A_{1g} Raman modes exhibit slight blue

shifts, reflecting a decrease of electron density (Fig. 1b) [41], which is consistent with the electrical characterization results (Fig. 1d).

Scanning probe and electrical characterizations

The AFM and PFM studies were carried out using a Bruker Multimode 8 AFM system. The AFM tip is SCM-PIC with a resonant frequency of ~ 170 kHz. The PFM measurements were performed using an AC voltage with a drive-amplitude of 300-500 mV at a frequency of 170 ± 20 kHz.

The electrical measurements were conducted at room temperature in a Quantum Design PPMS using external Keithley 2400 SourceMeters and the standard lock-in techniques. The reported electrical characterization results are based on six MoS₂ devices, denoted as D1-D6.

Acknowledgements:

We would like to thank David Ferry for insightful discussions, Dawei Li and Peter Kosch for experimental assistance, and Yongfeng Lu for the access to the Raman system. This work was supported by the Nebraska Materials Research Science and Engineering Center (MRSEC) (NSF Grant No. DMR-1420645) (ferroelectric deposition and device fabrication), NSF CAREER Grant No. DMR-1148783 (electrical characterization), and NSF Grant No. OIA-1538893 (scanning probe study). Part of the research utilized the central facilities of the Nebraska Center for Materials and Nanoscience, which is supported by the Nebraska Research Initiative.

Author Contributions:

X.H. conceived the experiments. Z.X. carried out the MoS₂ device fabrication, electrical characterization, and scanning probe studies. J.S. and S.D. prepared the ferroelectric polymer films. X.H. and Z.X. performed the data analysis. All authors discussed the results and contributed to the manuscript preparation.

References:

- [1] M. Mitchell Waldrop, The chips are down for Moore's law, *Nature* 530 (2016).
- [2] W. Lu, and C. M. Lieber, Nanoelectronics from the bottom up, *Nature Materials* 6, 841 (2007).
- [3] A. K. Geim, and I. V. Grigorieva, Van der Waals heterostructures, *Nature* 499, 419 (2013).
- [4] C. Cen, S. Thiel, J. Mannhart, and J. Levy, Oxide Nanoelectronics on Demand, *Science* 323, 1026 (2009).
- [5] X. Hong, Emerging ferroelectric transistors with nanoscale channel materials: the possibilities, the limitations, *Journal of Physics: Condensed Matter* 28, 103003 (2016).
- [6] Q. H. Wang, K. Kalantar-Zadeh, A. Kis, J. N. Coleman, and M. S. Strano, Electronics and optoelectronics of two-dimensional transition metal dichalcogenides, *Nature Nanotechnology* 7, 699 (2012).
- [7] B. Radisavljevic, and A. Kis, Mobility engineering and a metal-insulator transition in monolayer MoS₂, *Nature Materials* 12, 815 (2013).
- [8] Y. Yoon, K. Ganapathi, and S. Salahuddin, How Good Can Monolayer MoS₂ Transistors Be?, *Nano Letters* 11, 3768 (2011).
- [9] B. Radisavljevic, A. Radenovic, J. Brivio, V. Giacometti, and A. Kis, Single-layer MoS₂ transistors, *Nature Nanotechnology* 6, 147 (2011).
- [10] D. Jariwala, V. K. Sangwan, L. J. Lauhon, T. J. Marks, and M. C. Hersam, Emerging Device Applications for Semiconducting Two-Dimensional Transition Metal Dichalcogenides, *Acs Nano* 8, 1102 (2014).
- [11] W. J. Zhu, T. Low, Y. H. Lee, H. Wang, D. B. Farmer, J. Kong, F. N. Xia, and P. Avouris, Electronic transport and device prospects of monolayer molybdenum disulphide grown by chemical vapour deposition, *Nature Communications* 5, 3087 (2014).
- [12] Z. Yin, H. Li, H. Li, L. Jiang, Y. Shi, Y. Sun, G. Lu, Q. Zhang, X. Chen, and H. Zhang, Single-Layer MoS₂ Phototransistors, *ACS Nano* 6, 74 (2012).
- [13] F. H. L. Koppens, T. Mueller, P. Avouris, A. C. Ferrari, M. S. Vitiello, and M. Polini, Photodetectors based on graphene, other two-dimensional materials and hybrid systems, *Nature Nanotechnology* 9, 780 (2014).
- [14] B. W. H. Baugher, H. O. H. Churchill, Y. F. Yang, and P. Jarillo-Herrero, Optoelectronic devices based on electrically tunable p-n diodes in a monolayer dichalcogenide, *Nature Nanotechnology* 9, 262 (2014).
- [15] D. J. Groenendijk, M. Buscema, G. A. Steele, S. M. de Vasconcellos, R. Bratschitsch, H. S. J. van der Zant, and A. Castellanos-Gomez, Photovoltaic and Photothermoelectric Effect in a Double-Gated WSe₂ Device, *Nano Letters* 14, 5846 (2014).
- [16] S. Jo, N. Ubrig, H. Berger, A. B. Kuzmenko, and A. F. Morpurgo, Mono- and Bilayer WS₂ Light-Emitting Transistors, *Nano Letters* 14, 2019 (2014).
- [17] S. Chuang, C. Battaglia, A. Azcatl, S. McDonnell, J. S. Kang, X. Yin, M. Tosun, R. Kapadia, H. Fang, R. M. Wallace, and A. Javey, MoS₂ P-type Transistors and Diodes Enabled by High Work Function MoO_x Contacts, *Nano Letters* 14, 1337 (2014).
- [18] J. Wang, D. Rhodes, S. Feng, M. A. T. Nguyen, K. Watanabe, T. Taniguchi, T. E. Mallouk, M. Terrones, L. Balicas, and J. Zhu, Gate-modulated conductance of few-layer WSe₂ field-effect transistors in the subgap regime: Schottky barrier transistor and

- subgap impurity states, *Applied Physics Letters* 106, 152104 (2015).
- [19] C. H. Lee, G. H. Lee, A. M. van der Zande, W. C. Chen, Y. L. Li, M. Y. Han, X. Cui, G. Arefe, C. Nuckolls, T. F. Heinz, J. Guo, J. Hone, and P. Kim, Atomically thin p-n junctions with van der Waals heterointerfaces, *Nature Nanotechnology* 9, 676 (2014).
- [20] Y. X. Deng, Z. Luo, N. J. Conrad, H. Liu, Y. J. Gong, S. Najmaei, P. M. Ajayan, J. Lou, X. F. Xu, and P. D. Ye, Black Phosphorus-Monolayer MoS₂ van der Waals Heterojunction p-n Diode, *Acs Nano* 8, 8292 (2014).
- [21] M. M. Furchi, A. Pospischil, F. Libisch, J. Burgdörfer, and T. Mueller, Photovoltaic Effect in an Electrically Tunable van der Waals Heterojunction, *Nano Letters* 14, 4785 (2014).
- [22] F. Withers, O. Del Pozo-Zamudio, A. Mishchenko, A. P. Rooney, A. Gholinia, K. Watanabe, T. Taniguchi, S. J. Haigh, A. K. Geim, A. I. Tartakovskii, and K. S. Novoselov, Light-emitting diodes by band-structure engineering in van der Waals heterostructures, *Nature Materials* 14, 301 (2015).
- [23] H. S. Lee, S. W. Min, M. K. Park, Y. T. Lee, P. J. Jeon, J. H. Kim, S. Ryu, and S. Im, MoS₂ Nanosheets for Top-Gate Nonvolatile Memory Transistor Channel, *Small* 8, 3111 (2012).
- [24] A. Nguyen, P. Sharma, T. Scott, E. Preciado, V. Klee, D. Sun, I. H. D. Lu, D. Barroso, S. Kim, V. Y. Shur, A. R. Akhmatkhanov, A. Gruverman, L. Bartels, and P. A. Dowben, Toward Ferroelectric Control of Monolayer MoS₂, *Nano letters* 15, 3364 (2015).
- [25] C. Zhou, X. Wang, S. Raju, Z. Lin, D. Villaroman, B. Huang, H. L.-W. Chan, M. Chan, and Y. Chai, Low voltage and high ON/OFF ratio field-effect transistors based on CVD MoS₂ and ultra high-k gate dielectric PZT, *Nanoscale* 7, 8695 (2015).
- [26] H. Lu, A. Lipatov, S. Ryu, D. J. Kim, H. Lee, M. Y. Zhuravlev, C. B. Eom, E. Y. Tsymlal, A. Sinitskii, and A. Gruverman, Ferroelectric tunnel junctions with graphene electrodes, *Nature Communications* 5, 5518 (2014).
- [27] W. Park, J. H. Yang, C. G. Kang, Y. G. Lee, H. J. Hwang, C. Cho, S. K. Lim, S. C. Kang, W. K. Hong, S. K. Lee, S. Lee, and B. H. Lee, Characteristics of a pressure sensitive touch sensor using a piezoelectric PVDF-TrFE/MoS₂ stack, *Nanotechnology* 24, 475501 (2013).
- [28] A. Rajapitamahuni, J. Hoffman, C. H. Ahn, and X. Hong, Examining Graphene Field Effect Sensors for Ferroelectric Thin Film Studies, *Nano Letters* 13, 4374 (2013).
- [29] C. Ma, Y. Gong, R. Lu, E. Brown, B. Ma, J. Li, and J. Wu, Detangling Extrinsic and Intrinsic Hysteresis for Detecting Dynamic Switch of Electric Dipoles using Graphene Field-Effect Transistors on Ferroelectric Gates, *Nanoscale* (2015).
- [30] M. D. Goldflam, G.-X. Ni, K. W. Post, Z. Fei, Y. Yeo, J. Y. Tan, A. S. Rodin, B. C. Chapler, B. Özyilmaz, A. H. Castro Neto, M. M. Fogler, and D. N. Basov, Tuning and Persistent Switching of Graphene Plasmons on a Ferroelectric Substrate, *Nano Letters* 15, 4859 (2015).
- [31] A. Lipatov, P. Sharma, A. Gruverman, and A. Sinitskii, Optoelectrical Molybdenum Disulfide (MoS₂)—Ferroelectric Memories, *ACS Nano* 9, 8089 (2015).
- [32] X. Wang, P. Wang, J. Wang, W. Hu, X. Zhou, N. Guo, H. Huang, S. Sun, H. Shen, T. Lin, M. Tang, L. Liao, A. Jiang, J. Sun, X. Meng, X. Chen, W. Lu, and J. Chu, Ultrasensitive and Broadband MoS₂ Photodetector Driven by Ferroelectrics, *Advanced*

- Materials 27, 6575 (2015).
- [33] S. Ducharme, S. P. Palto, V. M. Fridkin, and L. M. Blinov, in *Handbook of Thin Film Materials*, edited by H. S. Nalwa (Academic, San Diego, 2002).
 - [34] M. J. Bai, A. V. Sorokin, D. W. Thompson, M. Poulsen, S. Ducharme, C. M. Herzinger, S. Palto, V. M. Fridkin, S. G. Yudin, V. E. Savchenko, and L. K. Gribova, Determination of the optical dispersion in ferroelectric vinylidene fluoride (70%)/trifluoroethylene (30%) copolymer Langmuir-Blodgett films, *Journal of Applied Physics* 95, 3372 (2004).
 - [35] Z. Xiao, S. Poddar, S. Ducharme, and X. Hong, Domain wall roughness and creep in nanoscale crystalline ferroelectric polymers, *Applied Physics Letters* 103, 112903 (2013).
 - [36] Z. Xiao, J. Hamblin, S. Poddar, S. Ducharme, P. Paruch, and X. Hong, Effect of thermal annealing on ferroelectric domain structures in poly(vinylidene-fluoride-trifluoroethylene) Langmuir-Blodgett thin films, *Journal of Applied Physics* 116, 066819 (2014).
 - [37] T. Jin, J. Kang, E. S. Kim, S. Lee, and C. Lee, Suspended single-layer MoS₂ devices, *Journal of Applied Physics* 114 (2013).
 - [38] N. Ma, and D. Jena, Charge Scattering and Mobility in Atomically Thin Semiconductors, *Physical Review X* 4, 011043 (2014).
 - [39] D. K. Schroder, *Semiconductor Material and Device Characterization* (John Wiley & Sons, Inc, Hoboken, New Jersey, 2006).
 - [40] J. Kunc, Y. K. Hu, J. Palmer, Z. L. Guo, J. Hankinson, S. H. Gamal, C. Berger, and W. A. de Heer, Planar Edge Schottky Barrier-Tunneling Transistors Using Epitaxial Graphene/SiC Junctions, *Nano Letters* 14, 5170 (2014).
 - [41] B. Chakraborty, A. Bera, D. V. S. Muthu, S. Bhowmick, U. V. Waghmare, and A. K. Sood, Symmetry-dependent phonon renormalization in monolayer MoS₂ transistor, *Physical Review B* 85 (2012).

Figure 1

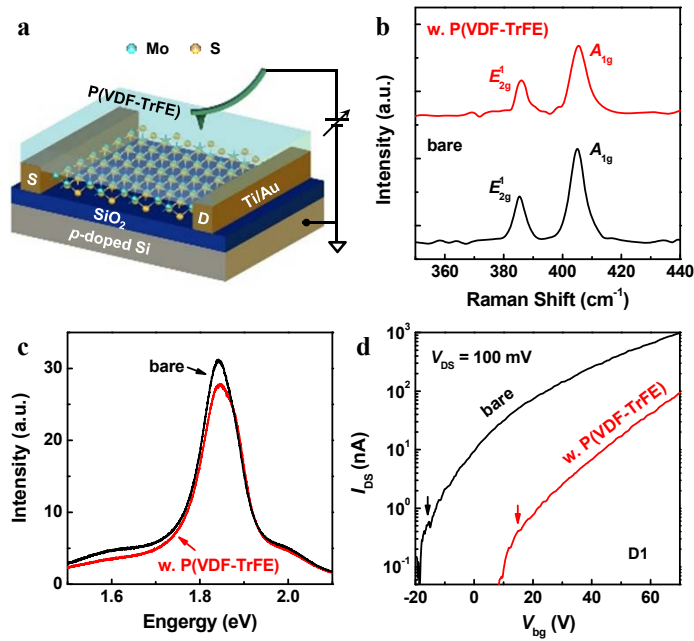


Fig. 1. Device fabrication and characterization. (a) Schematic view of a MoS₂ FET sandwiched between a P(VDF-TrFE) top-gate and a SiO₂ back-gate. Voltage is applied to a conductive AFM tip to write and image the domain structures in the ferroelectric polymer. (b) Raman and (c) PL spectra of a ML MoS₂ flake before (bare) and after the deposition of the ferroelectric top layer. (d) Room-temperature I_{DS} - V_{bg} for device D1 before and after the ferroelectric polymer deposition. The arrows mark the corresponding V_{ts} .

Figure 2

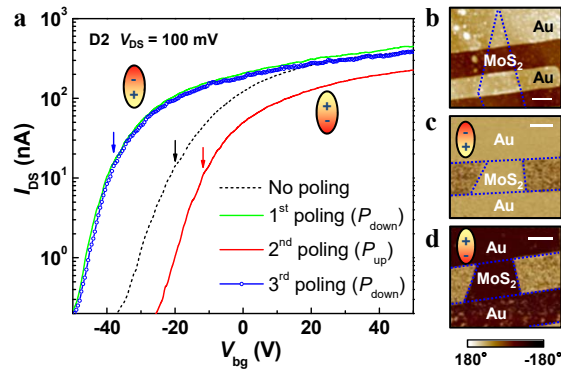


Fig. 2. Effect of ferroelectric polarization on MoS₂ FET. (a) Room-temperature transfer characteristics for device D2 in the initial no poling state, and after writing the copolymer top layer with +10 V (1st poling), -10 V (2nd poling), and +10 V (3rd poling) tip bias, resulting in the P_{down} , P_{up} , and P_{down} domains, respectively. The arrows mark the corresponding V_{ts} . (b) The AFM topography image of the device and the PFM phase images after (c) the 1st and (d) 2nd poling. The scale bars are 1 μm . The dotted lines outline the MoS₂ flake and the Au electrodes.

Figure 3

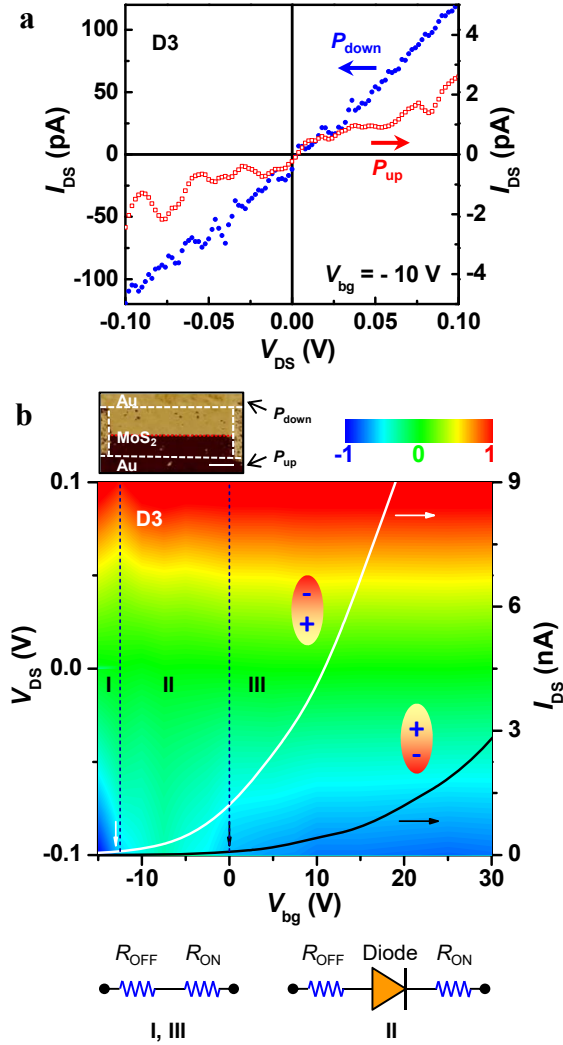


Fig. 3. Conduction characteristics of MoS₂ FET with different top-gate domain structures. (a) Room-temperature I_{DS} - V_{DS} of device D3 for the uniform P_{up} and P_{down} states at $V_{bg} = -10$ V. (b) Normalized I_{DS} vs. V_{DS} and V_{bg} for device D3 for the half P_{up} -half P_{down} state. Superimposed on the plot are the transfer curves at $V_{DS} = 100$ mV for the uniform P_{up} and P_{down} states (right axis). The vertical arrows mark the $V_{t,s}$. The dashed lines mark the boundaries separating regions I, II, and III. Insets: (Top) PFM phase image of the half P_{up} -half P_{down} domain structure. Scale bar: 1 μ m. (Bottom) Schematics of the equivalent circuit elements for different regions.

Figure 4

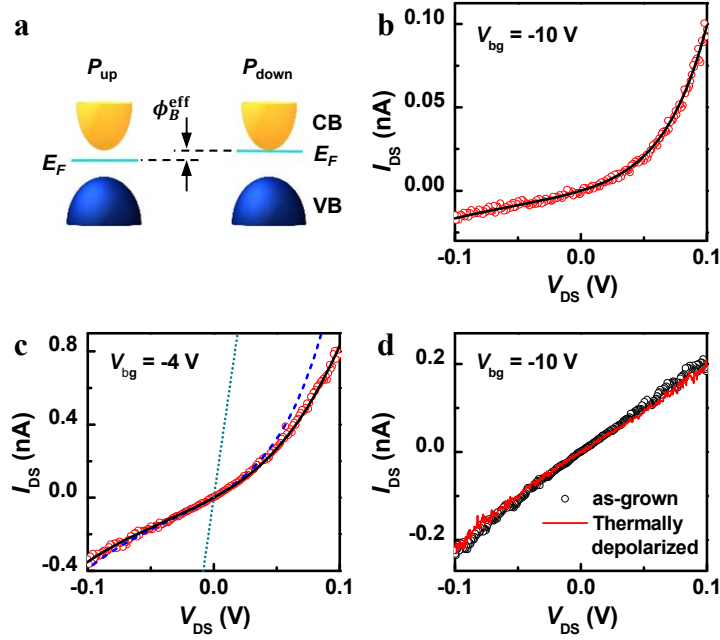


Fig. 4. Ferroelectric domain patterning induced diode state. (a) Schematic band diagram for MoS₂ in the P_{up} and P_{down} states. (b)-(d) Conduction characteristics for device D4 in region II. (b) $I_{\text{DS}}-V_{\text{DS}}$ (open symbols) at $V_{\text{bg}} = -10$ V with a fit to Eq. (1) (solid line). (c) $I_{\text{DS}}-V_{\text{DS}}$ (open symbols) at $V_{\text{bg}} = -4$ V with a fit to Eq. (2) (solid line). The dashed and dotted lines correspond to the first and second terms in Eq. (2), respectively. (d) $I_{\text{DS}}-V_{\text{DS}}$ at $V_{\text{bg}} = -10$ V taken in the as-grown state of P(VDF-TrFE) (black symbols) and after domain patterning and thermal depolarization (red line).

Figure 5

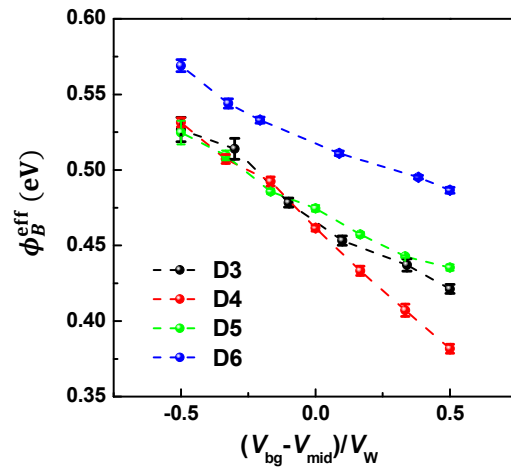


Fig. 5. Back-gate tuning of Schottky barrier height. The effective Schottky barrier height for devices D3-D6 as a function of normalized V_{bg} .